Supplemental Material for "Persistence of a freshwater surface ocean after a snowball Earth"

Jun Yang, Malte F. Jansen, Francis A. Macdonald, and Dorian S. Abbot

METHODS

Estimating the Energy Input to Deep Ocean Mixing

To understand post-snowball mixing, we need to understand potential changes in the energy sources for vertical mixing. The largest energy source to deep ocean mixing arises from tidal flows (e.g., Waterhouse et al., 2014). Based on the analysis of sedimentary cyclic rhythmites of tidal origin, Williams (2000) suggested that the average rate of energy dissipation by the lunar tide since the cryogenic period was about 40% smaller than today[1]. **The present rate of tidal energy dissipation thus appears to be unusually large, likely due to resonances associated with the specific continental configuration (Green et a., 2017)**. **The moon was closer than today, but only by a few percent (<5%), which has a comparatively small effect.** As tidal energy dissipation has likely varied non-monotonically during the last 700 million years (e.g., due to changes in the continental configuration), the rate of tidal energy dissipation during the ice-free periods of the cryogenic itself is less well constraint, but much larger dissipation rates than today appear to be unlikely. Less than 50% of the total tidal energy dissipation is presently transferred into internal waves, which can break and contribute to vertical mixing in the ocean

[1] The average tidal energy dissipation can be inferred from the rate of change in the moon's orbital radius. The orbital radius has **increased** by an average of about 2.2 cm/year since the late Neoproterozoic, which corresponds to just over half the present rate, **3.8 cm/year** (e.g., Williams, 2000). Since total changes in the orbital radius over this time period have been relatively small (<~5%), the energy dissipation rate is approximately linearly proportional to the rate of change of the orbital radius.

interior (Wunsch and Ferrari, 2004). The rest is dissipated on shallow shelves or in the bottom boundary layer. The fraction of tidal energy that is transferred into internal waves depends primarily on the abyssal stratification and bottom topographic roughness (Jayne and St. Laurent, 2001). While the interior ocean would be highly stratified in the aftermath of a snowball Earth event, the abyss would likely lose its stratification relatively quickly (see Fig. 2 in the main text), thus potentially making the conversion of tidal energy much less efficient. Topographic roughness is controlled largely by tectonic processes, and is unlikely to have changed very much. In the following, we assume the tidal power input to interior-ocean turbulence to be 60% of the present-day value of ~1.5 TW (TW: 10^{12} W; Waterhouse et al., 2014), i.e., 0.9 TW, but with a plausible range between 0.3-2.7 TW.

An additional source of energy for mixing arises from wind-driven near-inertial and geostrophic ocean currents. For the present-day, this energy input amounts to about 0.5 TW (Wunsch and Ferrari, 2004; Waterhouse et al., 2014). Due to the very small equator-to-pole surface temperature difference (Fig. 1 in the main text) after the snowball, surface wind stresses over the ocean would likely be smaller than today, as can be seen in simulations using a 3D atmospheric circulation model (Fig. DR1 below). The result suggests a reduction in wind energy input. Assuming that surface current speeds are to first order proportional to the magnitude of the wind stress, the total wind work is expected to scale with the square of the wind stress, which in turn is estimated to be reduced to ~60% of today's value. In the following, we assume a wind-driven power input to interior ocean turbulence of 0.3 TW, with a large uncertainty range of 0.1-0.9 TW. We therefore estimate the total interior turbulent dissipation (ε) as ~1.2 TW, with an uncertainty range between 0.4 and 3.6 TW. Notice that we conservatively added uncertainties for tidal and wind-driven energy dissipation linearly.

The mixing efficiency Γ is generally assumed to be 0.2, based on Osborn (1980). Theoretical and experimental studies show that the value of Γ depends non-monotonically on the local Richardson number (Peltier and Caulfield, 2003), but we have little reason to believe that the average mixing efficiency has changed substantially between the present and post-snowball climates. Moreover, a much larger value than the canonical $\Gamma = 0.2$ can be excluded on theoretical and experimental grounds (Ivey et al., 2008). Here we assume $\Gamma = 0.2$, with an uncertainty range between 0.1 and 0.3. This yields an energy input to vertical mixing of $\Gamma \times \varepsilon = 1.2 \times 0.2 \sim 0.3$ TW, with a conservative uncertainty range between 0.04 and 1.1 TW.

1-D Mixing Model Setup

We integrate the 1D mixing equation (Eq. (3) of the main text) with an initial state of a 2-km deep layer of cold and salty water. In the control run, we add a 2-km freshwater layer at a constant rate of 2 m per year. The potential temperature, salinity, and diffusion coefficient at the time right after all of the freshwater has entered the ocean are shown in Fig. 1 (blue lines) of the main text. We prescribe a fixed vertical structure for the diffusion coefficient, which is enhanced near the surface and at the ocean bottom to account for the effects of surface winds and bottom topography, respectively (Fig. 1D). The magnitude of the eddy diffusivity evolves in time and is computed following Eq. (1) of the main text, with a fixed energy input rate $\Gamma \times \varepsilon$. For very small N^2, the diffusion coefficient will be large enough to induce numerical instability. We avoid this by introducing an upper limit of 0.01 $m^2\ s^{-1}$. This has a very small effect on the result, since N^2 becomes small during the final stage of the simulation. We also include a lower limit of 10^{-7} $m^2\ s^{-1}$, which corresponds to the molecular diffusivity of heat.

When the density profile is unstable with dense water overlying light water, convection will occur, which is parameterized by setting the diffusion coefficient to a large value of 0.01 m^2 s^{-1}, as is done in global ocean circulation models (e.g., Smith et al., 2010). In our calculations, convection mostly occurs near the bottom of the ocean, where the geothermal heat flux acts to destabilize the seawater. The ocean has a depth of 4 km with 21 vertically uniform levels. The time step is 0.025 year. The equation of state of seawater employed here and in METHOD I of the main text is that of Millero and Huang (2009), which is valid for wide ranges of salinity (5 to 70 g kg^{-1}) and potential temperature (0 to 90 ^{o}C).

During the evolution of the post-snowball ocean, the change of vertical diffusivity is not a monotonic function of time, particularly during the phase of freshwater addition (see Fig. 2D of the main text). In the snowball state and at the beginning of the melting, the ocean has nearly uniform salinity (about 66 g kg^{-1}) and uniform temperature (close to the freezing point), thus, vertical stratification is weak and the diffusivity is large, close to the convection limit of 0.01 m^2 s^{-1}. When freshwater is added to the ocean, stratification increases and the diffusivity decreases. At the time when all of the freshwater has been added to the ocean, vertical stratification reaches its maximum and the diffusivity reaches its minimum. After that, the ocean mixing acts to decrease the stratification, so that the diffusivity increases with time, according to Eq (1) in the main text. Sensitivity tests show that the detailed evolutions of diffusivity and sea surface temperature in the phase of freshwater addition have no significant effect on the bulk timescale estimates and have a small effect (<5 m) on the magnitude of sea level rise associated with pure thermal expansion.

In the model, the surface temperature is fixed to 50 ^{o}C after all of the freshwater has entered the ocean. This is based on the result of a 3D global climate model, CAM3. The

model solves the primitive equations of atmospheric motion on a rotating sphere and the equations for realistic radiative transfer and parameterized convection, condensation, precipitation, clouds, and boundary turbulence (Collins et al., 2004; Boville et al., 2006). It is a standard model that climate scientists employ for simulating the climates of Earth in the past, present, and future. Different types of climate models, including energy balance models (Hoffman and Schrag, 2002; Pierrehumbert et al., 2011) and a 3D global climate model (Le Hir et al., 2008), have also been employed to estimate the post-snowball surface temperature. All of these models found that the post-snowball surface temperature is 50 ^{o}C or greater due to the high concentration of atmospheric CO_2 and strong water vapor feedback.

Based on the estimation of a combined climate-weathering model (Le Hir et al., 2008), the timescale of the silicate weathering cycle to decrease the post-snowball CO_2 concentration is 10^6 years, much longer than previously thought (such as Hoffman and Schrag, 2002). Although the surface temperature is high, continental runoff might be only ~1.2 times the modern runoff (Le Hir et al., 2008b). This is due to the fact that precipitation (and hence runoff) is limited by the supply of solar radiation absorbed at the surface, rather than the surface temperature (Pierrehumbert, 2002). The silicate weathering timescale (10^6 years) is about 10 times the maximum ocean mixing timescale estimated here (10^5 years), so that the assumption of fixed surface temperature of 50 ^{o}C in our model is reasonable.

Finally, we note that most present-day 3D ocean models are not suitable for simulating the post-snowball ocean, as spurious, non-physical numerical diffusion in the models (e.g., Griffies

et al., 2000) may be comparable to or even larger than the small diffusivity of the post-snowball ocean. This is the reason we develop a 1D mixing model.

REFERENCES

Boville, B.A., Rasch, P.J., Hack, J.J. & McCaa, J.R., 2006, Representation of clouds and precipitation processes in the Community Atmosphere Model version 3 (CAM3): J. Climate v. 19, p. 2162-2183.

Green, J.A.M., Huber, M., Waltham, D., Buzan, J., and Wells, M., 2017, Explicitly modelled deep-time tidal dissipation and its implication for Lunar history: Earth and Planetary Science Letters, v. 461, p. 46-53.

Griffies, S.M., Pacanowski, R.C., and Hallbergm R.W., 2000, Spurious Diapycnal Mixing Associated with Advection in a z-Coordinate Ocean Model: Monthly Weather Review, v. 128, p. 538-564, doi:10.1175/1520-0493(2000)128<0538:SDMAWA>2.0.CO;2.

Ivey, G.N., Winters, K.B., and Koseff, J.R., 2008, Density stratification, turbulence, but how much mixing? Annual Review of Fluid Mechanics, v. 40, no. 1, p. 169-184.

Jayne, S.R., and St Laurent, L.C., 2001, Parameterizing tidal dissipation over rough topography: Geophysical Research Letters, v. 28, no. 5, p. 811-814.

Le Hir, G., *et al.*, 2008b, The snowball Earth aftermath: Exploring the limits of continental weathering processes: Earth Planet. Sci. Lett., doi:10.1016/j.epsl.2008.11.010.

Millero, F.J., and Huang, F., 2009, The density of seawater as a function of salinity (5 to 70 g kg^{-1}) and temperature (273.15 to 363.15 K): Ocean Science, v. 5, p. 91-100.

Osborn, T.R., 1980, Estimates of the local rate of vertical diffusion from dissipation measurements: Journal of Physical Oceanography, v. 10, no. 1, p. 83-89.

Peltier, W.R., and Caulfield, C.P., 2003, Mixing Efficiency Stratified Shear Flows: Annual Review of Fluid Mechanics, v. 35, p. 135-167.

Pierrehumbert, R.T., 2002, The hydrologic cycle in deep-time climate problems: Nature, v. 419, p. 191–198.

Pierrehumbert, R.T., Abbot, D.S., Voigt, A., and Koll D.B. D., 2011, Climate of the Neoproterozoic: Annual Review of Earth and Planetary Sciences, v. 39, p. 417-460.

Smith, R., et al., 2010, The Parallel Ocean Program (POP) reference manual: Ocean component of the Community Climate System Model (CCSM): Los Alamos National Laboratory Report LAUR-10-01853, 140 p.

Williams, G.E., 2000, Geological constraints on the Precambrian history of Earth's rotation and the Moon's orbit, Rev. Geophys., v. 38, no. 1, p. 37–59.

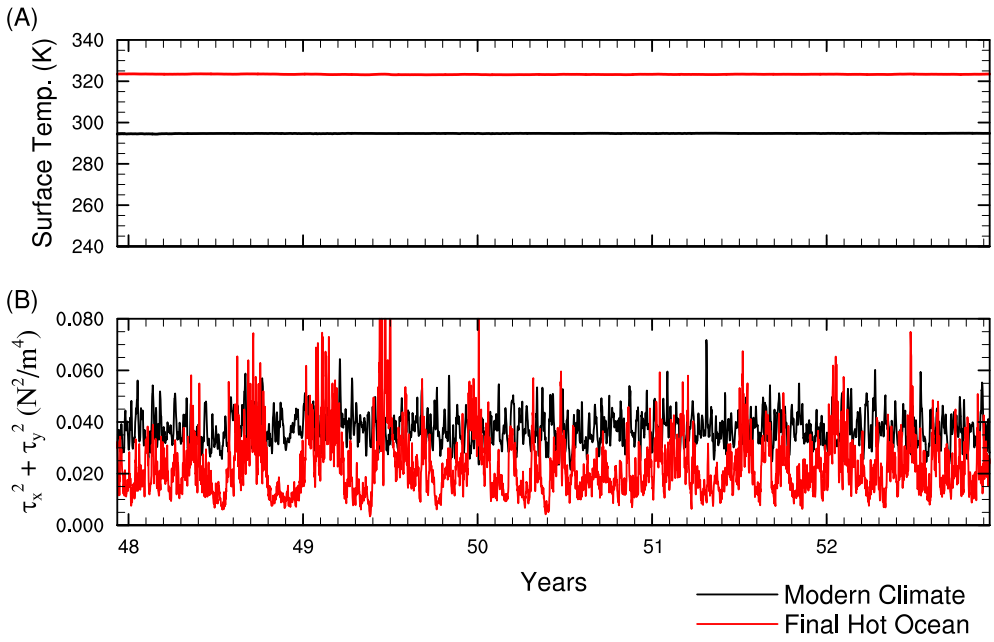

Figure DR1. Time series of global-mean surface temperature (A) and the square of surface wind stresses over oceans (B), simulated by the atmospheric circulation model CAM3. Black line: modern condition, and red line: the final equilibrium post-snowball ocean. The time interval is 12 hours in this plot. For a long-term mean, the global mean of the square of surface wind stresses in the post-snowball condition is about 60% of that in the modern condition, due to the fact that the meridional temperature gradients in the post-snowball condition are relatively weaker.

156

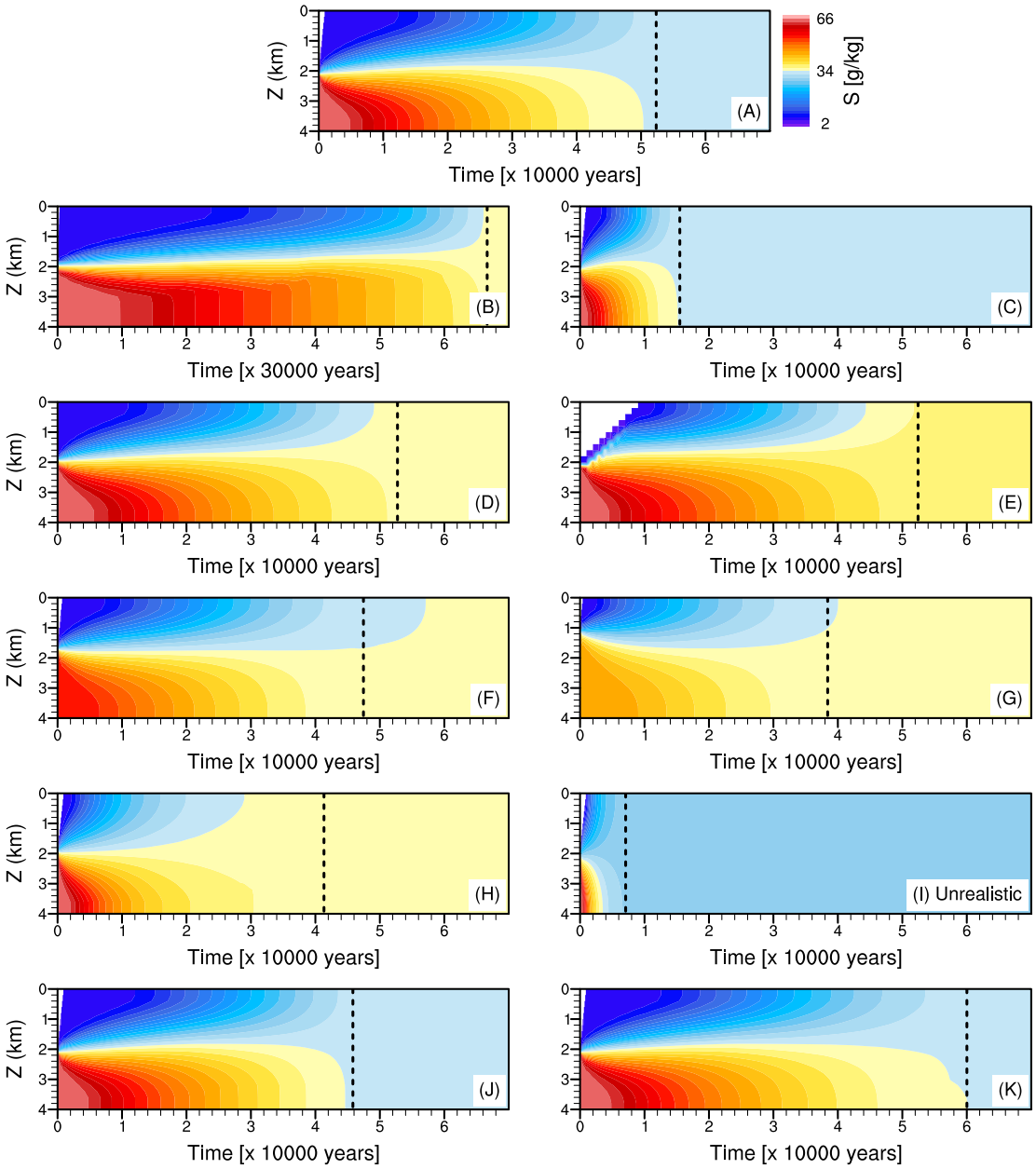

157

158 **Figure DR2: Evolution of ocean salinity of a post-snowball Earth under different**
159 **parameters. (A) The control experiment, same as Figure 2(A) in the main text for**
160 **comparison. (B) The mixing energy is 0.04 TW (versus 0.30 TW be default). (C) Same as B,**
161 **but for 1.10 TW. (D) The timescale of the freshwater entering the ocean is 100 years (versus**
162 **1000 years by default). (E) Same as D, but for 10,000 years. (F) The freshwater ocean depth**

is 1600 m (versus 2000 m by default). (G) Same as F, but for 1000 m. (H) The mixing coefficient is fixed to 6 x 10^{-6} m^2 s^{-1}. (I) Same as H, but for 3 x 10^{-5} m^2 s^{-1} (the modern Earth's mean value, but unrealistic for the post-snowball Earth). (J) The geothermal heat flux is 0.2 W m^{-2} (versus 0.1 W m^{-2} by default). (K) The geothermal heat flux is zero. The vertical dotted line denotes the time at which salinity becomes nearly uniform in depth (i.e., the difference of salinity between the sea surface and the ocean bottom is less than 1.0 g/kg). Note that the time interval in x-axis is 10,000 years in all of the panels except in (B) it is 30,000 years.